Measurement of the $\gamma p \rightarrow \pi^+ n$ Reaction near Threshold

E. Korkmaz,[1] N. R. Kolb,[2] D. A. Hutcheon,[3,4] G. V. O'Rielly,[1,5] J. C. Bergstrom,[2] G. Feldman,[5] D. Jordan,[4,6] A. K. Opper,[6] R. E. Pywell,[2] B. Sawatzky,[2] and D. M. Skopik[2]

[1]*Physics Department, University of Northern British Columbia, Prince George, British Columbia, Canada V2N 4Z9*
[2]*Saskatchewan Accelerator Laboratory, University of Saskatchewan, Saskatoon, Saskatchewan, Canada S7N 5C6*
[3]*TRIUMF, 4004 Wesbrook Mall, Vancouver, British Columbia, Canada V6T 2A3*
[4]*Physics Department, University of Alberta, Edmonton, Alberta, Canada V2L 5P2*
[5]*Physics Department, George Washington University, Washington, D.C. 20052*
[6]*Department of Physics and Astronomy, Ohio University, Athens, Ohio 45701*

(Received 29 July 1999)

Differential cross sections for the $\gamma p \rightarrow \pi^+ n$ reaction have been measured at photon energies 1 to 2 MeV above threshold using tagged-photon beams. The electric dipole amplitude E_{0+} deduced at threshold is compared to recent predictions from chiral perturbation theory. Constraints on the value of the πN coupling constant are inferred by combining theory and experiment.

PACS numbers: 25.20.Lj, 13.60.Le, 13.75.Gx

The renewed interest in threshold pion photoproduction from the nucleon has been manifested recently in both theory and experiment. Experimentally, the commissioning of new cw electron facilities with photon-tagging capabilities has allowed for a new generation of high quality measurements, free of the potentially large uncertainties associated with bremsstrahlung beams. Meanwhile, new theoretical techniques, specifically chiral perturbation theory (ChPT), have recently been applied to this process, resulting in corrections to the more traditional low-energy theorems based on current algebra and the partially conserved-axial-current hypothesis. These ChPT corrections [1] have now been confirmed by experiment [2,3] for the $\gamma p \rightarrow \pi^0 p$ reaction.

In this Letter we report the results of a cross-section measurement recently completed at the Saskatchewan Accelerator Laboratory (SAL), aimed at determining the threshold value of the *s*-wave amplitude, E_{0+}, of the $\gamma p \rightarrow \pi^+ n$ reaction. Previous measurements of this reaction [4] were performed with untagged bremsstrahlung beams and required extrapolation to threshold from relatively high energies since they all relied on the detection of the outgoing pions. In the present experiment, the recoil neutrons were detected instead in a segmented liquid-scintillator detector, utilizing the tagged-photon beam from the SAL facility and a liquid hydrogen (LH_2) target. A schematic of the experimental apparatus is shown in Fig. 1. Bremsstrahlung photons were tagged in the range 140–160 MeV (the reaction threshold is 151.44 MeV) by means of an electron tagging spectrometer equipped with a 62-channel focal plane detector array [5]. Two sets of measurements were made, one with a primary electron beam energy of 245 MeV, the other 293 MeV. The tagged photon resolutions (energy width per channel) for the two sets were 0.25 and 0.40 MeV, respectively.

Within 1–2 MeV of threshold, the reaction neutrons are emitted in a small forward cone in the laboratory system with kinetic energies between 6 and 14 MeV. The neutron detector [6], which consisted of an array of $847.6 \times 7.6 \times 6.4$ cm^3 rectangular cells of BC-505 liquid scintillator, was positioned 3 m downstream of the target, allowing for neutron detection between 1° and 8° with respect to the beam direction. Free passage of the incident photon beam was ensured by a hole in the detector at 0°. The neutron energies were measured by time-of-flight (TOF) with the tagger providing the photon hit time at the target. Measurement of neutron angle and energy allowed for an independent determination of the incident photon energy. Twelve plastic scintillator paddles were placed in front of the detector cells to serve as charged-particle vetos. Fast pulse-shape discrimination techniques [6] were employed to reject photon triggers. Further accidental neutron background was measured concurrently with the aid of the subthreshold tagger channels. The neutron signal-to-noise ratio was typically about two to one.

Figure 2 shows neutron yields vs reconstructed photon energy spectra for four selected tagger channels, where accidental background, measured with the subthreshold

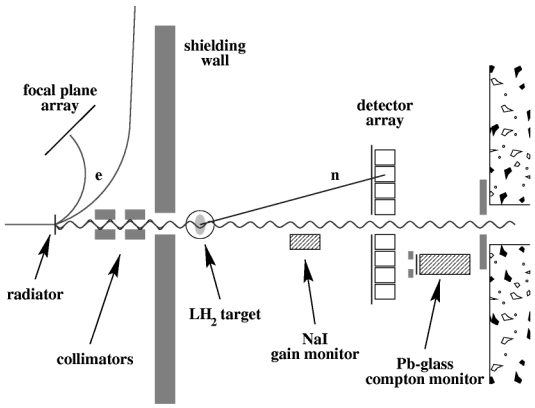

FIG. 1. Schematic of the $\gamma p \rightarrow \pi^+ n$ experimental apparatus (not to scale).

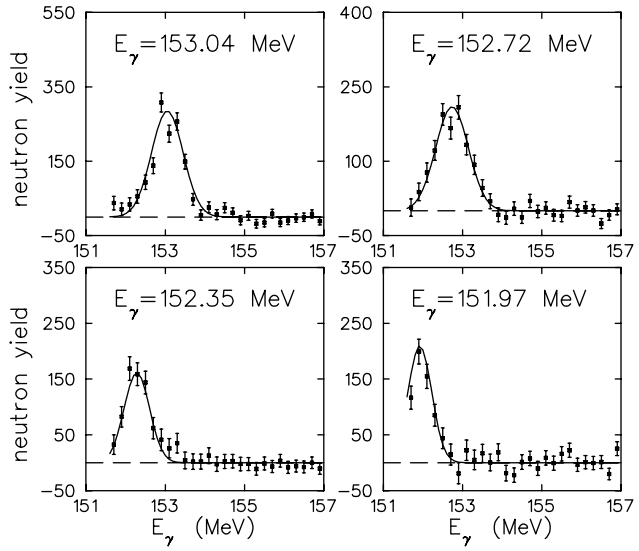

FIG. 2. Background-subtracted neutron yields at four photon energies just above the reaction threshold (151.44 MeV). The solid lines are the result of a simulation.

tagger channels and beam-flux normalized, has been subtracted. The photon energy reconstruction used the measured neutron energy and angle along with the $\gamma p \rightarrow \pi^+ n$ kinematics. Very clean peaks are observed in these spectra with typical energy resolution of 0.8 MeV (FWHM) reflecting the combined effect of the tagger channel width and neutron TOF and angle resolutions. The centroids of these peaks were determined to better than 40 keV.

The extraction of the absolute cross section at each photon energy (tagger channel) required knowledge of the absolute neutron detection efficiency, the LH_2 target thickness, and the flux of tagged photons hitting the target. The target thickness was measured during the experiment via Compton scattering with tagged photons normalized against two carbon targets of known thicknesses. The thickness thus determined was 5.77 ± 0.08 cm. This value was confirmed with a direct geometric measurement of the target cell appropriately pressurized, corrected for cell contraction at LH_2 temperature.

The photon flux incident on target was determined by tagger scalers and by frequent high-statistics measurements of the tagging efficiency at reduced electron beam current. The tagging efficiency is the ratio of detected electron-photon coincidences to electrons counted in the tagging spectrometer. The photons were detected with a large lead-glass counter positioned in the beam downstream of the target. Because of the tight collimation of the photon beam, the tagging efficiency was typically around 48%. The uncertainty in photon flux resulting from the statistics of these measurements is about 1.5%.

The absolute neutron detection efficiency at 8.9 MeV was measured [6] at TRIUMF using the neutron-tagging reaction (stopped $\pi^-)p \rightarrow n\gamma$. This was supplemented by a Monte Carlo simulation and measurements [6] of the detector pulse-height response to neutrons of different energies in the energy range of interest. Because of the sensitivity of the detection efficiency to the actual discriminator threshold on each cell, the gains of the photomultiplier tubes were continuously monitored during both the TRIUMF and SAL measurements using the Compton edge of ^{60}Co. The neutron yields and the detection efficiencies were extracted with a common software threshold of 0.8 MeV$_{ee}$ for all cells. We estimate the efficiencies thus determined to be accurate to within $\pm 2\%$ [6].

The input from the efficiency calibration was then used to generate the effective detector response function to neutrons from $\gamma p \rightarrow \pi^+ n$ for each tagger channel under the actual conditions of the experiment. The simulation assumed an isotropic neutron angular distribution in the center-of-mass system (consistent with *s*-wave pion production) and took into account the spatial and energy profiles of the tagged-photon beam, possible scattering of neutrons in the LH_2 target, the intrinsic efficiency of each cell, and possible side scattering between cells. Figure 3 shows the measured neutron angular distributions in terms of the neutron c.m. angle, along with the simulated detector response functions at four selected incident photon energies. The agreement in shape is very good and it is evident, for example, how more neutrons escape detection around 90° c.m. angle as the neutron forward cone opens up with increasing photon energy.

The reduced differential cross sections, $\frac{k}{q}\frac{d\sigma}{d\Omega}(\theta)$, were then extracted. Here, k is the photon momentum, q is the pion momentum, and θ is the pion angle, all in the c.m. system. Table I summarizes these cross sections at six photon energy bins spanning the first 2.2 MeV above

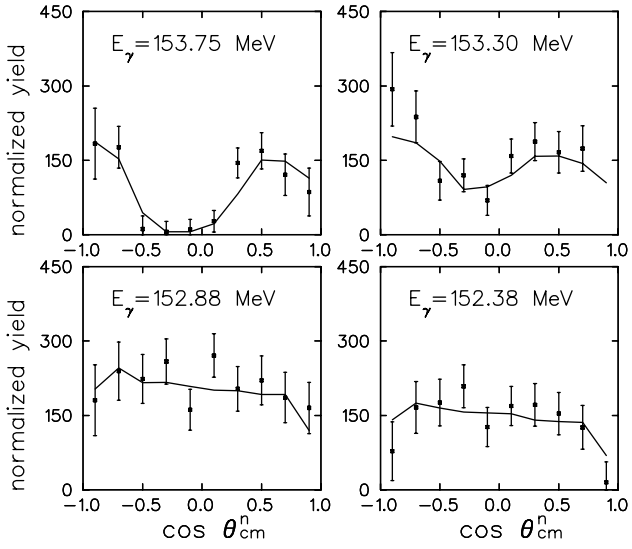

FIG. 3. Background-subtracted neutron yields at four photon energies close to threshold. Also shown (solid lines—normalized to fit the data) are the simulated detector response functions based on the measured detection efficiencies.

TABLE I. The reduced cross sections $\frac{k}{q}\frac{d\sigma}{d\Omega}(\theta^{\pi}_{\rm cm})$ (in μb/sr) at six photon energies close to threshold. Each energy bin is averaged over two or three tagger channels and has a typical width of 0.4–0.5 MeV. Threshold is at $E_\gamma = 151.44$ MeV.

$\cos\theta$	152.06 MeV	152.36	152.73
−0.7	9.3 ± 3.6	13.3 ± 4.7	15.0 ± 2.4
−0.5	13.3 ± 3.2	14.2 ± 2.8	14.3 ± 2.2
−0.3	12.0 ± 3.1	16.8 ± 2.8	15.8 ± 2.1
−0.1	15.6 ± 2.9	13.6 ± 2.4	19.2 ± 2.0
0.1	14.8 ± 2.9	11.7 ± 2.4	15.2 ± 1.9
0.3	16.7 ± 3.0	15.4 ± 2.5	19.5 ± 2.0
0.5	16.4 ± 4.8	16.6 ± 2.6	15.0 ± 2.1
0.7	15.5 ± 3.8	14.8 ± 2.7	15.0 ± 2.4

$\cos\theta$	153.06 MeV	153.39	153.75
−0.7	16.6 ± 2.7	15.5 ± 2.3	11.7 ± 2.4
−0.5	17.1 ± 2.5	14.8 ± 1.9	16.2 ± 2.1
−0.3	14.0 ± 2.1	18.5 ± 1.9	22.9 ± 3.1
−0.1	19.5 ± 2.2	17.0 ± 2.5	···
0.1	15.7 ± 2.4	13.6 ± 3.0	···
0.3	11.3 ± 2.0	12.9 ± 3.2	···
0.5	15.8 ± 2.2	10.6 ± 2.2	16.1 ± 3.1
0.7	16.9 ± 2.7	18.5 ± 2.1	15.7 ± 2.3

threshold. Each energy bin is averaged over two or three tagger channels. The angular distributions at four individual tagger energies are shown in Fig. 4. While results from different tagger channels were combined to produce a compact summary of our cross sections in Table I, we stress that our analysis was carried out entirely on an individual tagger channel basis.

The *s*- and *p*-wave amplitudes that contribute to $\gamma N \to \pi N$ are shown in Table II. At energies close to the reaction threshold, the cross section is dominated by these amplitudes and can be parametrized as

$$\frac{k}{q}\frac{d\sigma}{d\Omega} = [A + B\cos\theta + C\cos^2\theta]. \qquad (1)$$

In terms of the so-called natural *p*-wave amplitudes $P_1 = 3E_{1+} + M_{1+} - M_{1-}$, $P_2 = 3E_{1+} - M_{1+} + M_{1-}$, and $P_3 = 2M_{1+} + M_{1-}$, the coefficients *A*, *B*, and *C* are

$$\begin{aligned} A &= |E_{0+}|^2 + |P_{23}|^2, \\ B &= 2\,\mathrm{Re}(E_{0+}P_1^*), \\ C &= |P_1|^2 - |P_{23}|^2, \end{aligned} \qquad (2)$$

where $|P_{23}|^2 = \frac{1}{2}|P_2|^2 + \frac{1}{2}|P_3|^2$.

Within 1–2 MeV of threshold, the contribution of the *p*-wave amplitudes is expected to be very small compared to the *s*-wave. Neglecting the *p* waves, Eq. (1) becomes

$$\frac{k}{q}\frac{d\sigma}{d\Omega} = |E_{0+}|^2, \qquad (3)$$

implying flat angular distributions. Equation (3) was then used to fit the data. The fits at four photon energies are shown as the dashed lines in Fig. 4. The values of E_{0+} extracted for 18 individual tagger channels are plotted in Fig. 5 as a function of photon energy. In

TABLE II. The multipole amplitudes, up to *p*-wave pions, that contribute to the reaction $\gamma N \to \pi N$.

$l_{\pi N}$	J^π	L	Amplitude	Multipole
0	$\frac{1}{2}-$	1	E_{0+}	electric dipole
1	$\frac{3}{2}+$	1	M_{1+}	magnetic dipole
1	$\frac{1}{2}+$	1	M_{1-}	magnetic dipole
1	$\frac{3}{2}+$	2	E_{1+}	electric quadrupole

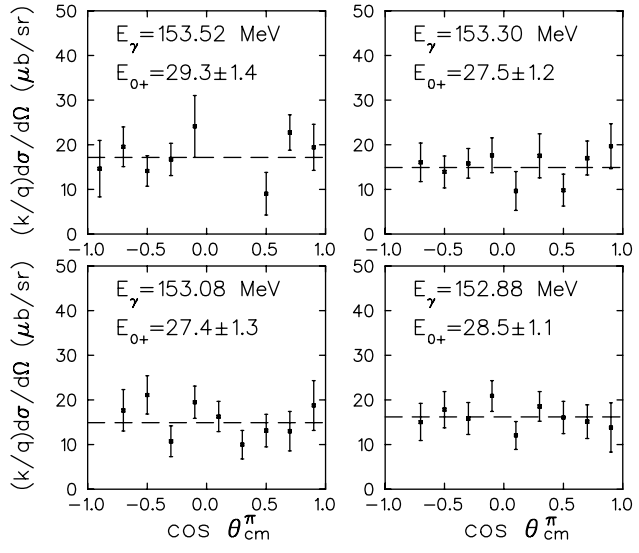

FIG. 4. The $\gamma p \to \pi^+ n$ differential cross sections at four photon energies close to threshold. The dashed lines are the fits obtained using Eq. (3). The corresponding values of E_{0+} in units of $10^{-3}m_\pi^{-1}$ are also shown.

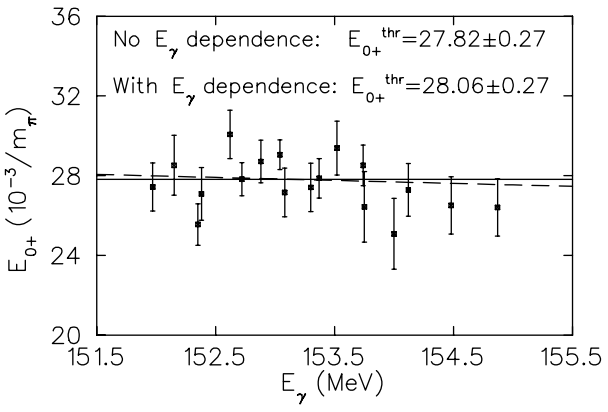

FIG. 5. The E_{0+} amplitudes for energies close to threshold. The values at threshold obtained under two different assumptions are also shown: the solid line has no E_γ dependence, while the dashed line has a fixed slope of 0.15 MeV^{-1}.

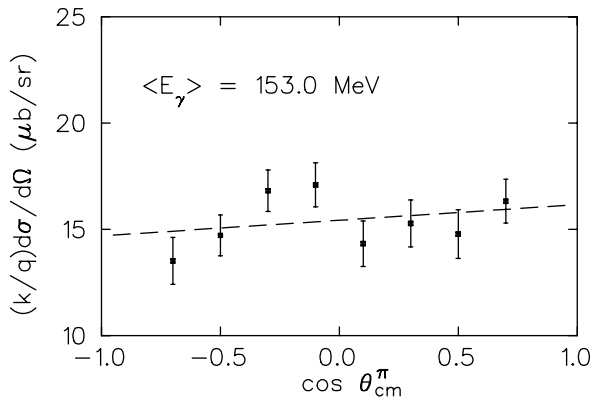

FIG. 6. The $\gamma p \to \pi^+ n$ differential cross section at an average photon energy of 153.0 MeV obtained by adding data from many tagger channels. The dashed line is a two-parameter fit using Eq. (1) with C set to zero.

Fig. 5, and throughout this Letter, E_{0+} is expressed in the conventional units of $10^{-3}m_\pi^{-1}$.

Assuming E_{0+} to be constant in the narrow energy range covered, the data in Fig. 5 were fitted and a value of $E_{0+} = 27.82 \pm 0.27$ obtained. However, this amplitude is believed, theoretically, to have a definite energy dependence dictated primarily by the dominant elementary Born amplitudes. In our energy range, it has been suggested [7], based on a dispersion partial-wave analysis of pion photoproduction, that E_{0+} should increase by 0.15 per MeV as threshold is approached. Refitting with this energy dependence leads to a threshold value of $E_{0+} = 28.06 \pm 0.27$. An independent linear fit with two free parameters leads to a slope of 0.29 ± 0.39 per MeV with an E_{0+} threshold value of 28.29 ± 0.70.

In order to test the s-wave-only assumption, a single higher-statistics angular distribution was obtained by adding together all the data shown in Table I. This distribution, which corresponds to an average photon energy of 153.0 MeV, is shown in Fig. 6. A fit was then carried out using Eq. (1) with parameter C set to zero (C is a pure p-wave term, whereas B is an s-p interference term). The following results were found (in units of μb): $A = 15.42 \pm 0.37$ and $B = 0.73 \pm 0.81$. Near threshold, all the amplitudes can safely be assumed to be real because of the very small πN phase shifts at these low pion energies. Equations (2) were then used along with the fitted A and B values to infer E_{0+} and P_1. We find the following (in units of $10^{-3}m_\pi^{-1}$): $E_{0+} = 27.85 \pm 0.33$ and $P_1 = 0.66 \pm 0.73$. This value of E_{0+} is fully consistent with the value obtained under the s-wave-only assumption at this average photon energy. The insensitivity of E_{0+} to the inclusion of the p-wave amplitudes in the fit is the result of the small B/A ratio ($4.7 \pm 5.3 \times 10^{-2}$). We note finally that the value of P_1 translates into 4.9 ± 5.4 in the conventional units of $10^{-3}(qk)/m_\pi^3$.

Our estimate of the systematic uncertainty on the reduced cross sections is 3.2%, obtained by a quadratic sum of uncertainties on the target thickness (1.4%), incident photon flux (1.5%), absolute neutron detection efficiency (2.0%), and central photon beam energy of each tagger channel (1.5% on the value of q/k). This translates into a systematic uncertainty on E_{0+} of 1.6% or ± 0.45. Our E_{0+} value at threshold, then, is

$$E_{0+}^{\text{thr}} = (28.06 \pm 0.27 \pm 0.45) \times 10^{-3}m_\pi^{-1}, \quad (4)$$

where the first error is statistical and the second systematic. This value is in agreement with the traditionally accepted value of Ref. [4] (27.9 ± 0.5) and the ChPT prediction of Ref. [8] (28.2 ± 0.6).

Because of the fast convergence of the chiral series for the $\gamma p \to \pi^+ n$ reaction [8], a combination of the final experimental value of E_{0+} and its ChPT value provides an opportunity to impose constraints on the πN coupling constant, whose value remains a topic of debate. This is the case because E_{0+} is directly proportional to $f_{\pi N}$ [8]. The ChPT prediction of Ref. [8] assumes the standard value $f_{\pi N}^2 = 0.079$. Full agreement between our result and ChPT is obtained with $f_{\pi N}^2 = 0.078 \pm 0.003$. This is more in accord with the standard value than with the more recently advertised value of 0.075 ± 0.001 favored by some analyses of NN and πN scattering data [9].

In summary, differential cross sections for $\gamma p \to \pi^+ n$ have been measured at photon energies within 1–2 MeV of the reaction threshold. Using an energy-dependent fit for the electric dipole amplitudes, a threshold value of $E_{0+} = (28.06 \pm 0.27) \times 10^{-3}m_\pi^{-1}$ is found, with a systematic uncertainty estimated at ± 0.45. This value is in agreement with the ChPT prediction of 28.2 ± 0.6 using 0.079 for $f_{\pi N}^2$.

[1] V. Bernard, N. Kaiser, and Ulf-G. Meißner, Z. Phys. C **70**, 483 (1996).
[2] J. C. Bergstrom *et al.*, Phys. Rev. C **53**, R1052 (1996); J. C. Bergstrom, R. Igarashi, and J. M. Vogt, Phys. Rev. C **55**, 2016 (1997); J. C. Bergstrom, Phys. Rev. C **58**, 2574 (1998).
[3] M. Fuchs *et al.*, Phys. Lett. B **368**, 20 (1996); A. M. Bernstein *et al.*, Phys. Rev. C **55**, 1509 (1997).
[4] M. I. Adamovitch, Proc. P. N. Lebedev Phys. Inst. **71**, 119 (1976), and references therein.
[5] J. M. Vogt *et al.*, Nucl. Instrum. Methods Phys. Res., Sect. A **324**, 198 (1993).
[6] E. Korkmaz *et al.*, Nucl. Instrum. Methods Res., Sect. A **431**, 446 (1999); B. Sawatzky, M.Sc. thesis, University of Saskatchewan, 1999 (unpublished).
[7] O. Hanstein, D. Drechsel, and L. Tiator, Nucl. Phys. **A632**, 561 (1998); L. Tiator (private communication).
[8] V. Bernard, N. Kaiser, and Ulf-G. Meißner, Phys. Lett. B **383**, 116 (1996).
[9] See, for example, R. G. E. Timmermans, π-N Newsletter **13**, 80 (1997).